Conditions for CET in a gamma TiAl alloy

2015 IOP Conf. Ser.: Mater. Sci. Eng. 84 012088

(http://iopscience.iop.org/1757-899X/84/1/012088)

Conditions for CET in a gamma TiAl alloy

R P Mooney[1], J Lapin[2], A Klimová[2] and S McFadden[1]

[1] Trinity College Dublin, Dublin 2, Ireland.
[2] Institute of Materials and Machine Mechanics, Slovak Academy of Sciences, Racianska 75, 831 02 Bratislava, Slovak Republic.

Email: Shaun.McFadden@tcd.ie

Abstract. The solidification of gamma TiAl alloys is of interest to the aerospace and automotive industries. A gamma TiAl multicomponent alloy: Ti–45.5Al–4.7Nb–0.2C–0.2B (at. %) has been the focus of a study to investigate the solidification conditions that led to a Columnar to Equiaxed Transition (CET) in a directional solidification experiment where traditional Bridgman solidification was combined in series with the power down method. In this paper, a numerical modelling result (a locus plot of columnar growth rate and temperature gradient) from this experiment is superimposed onto CET maps generated using an established analytical model for CET from the literature. A parametric study is carried out over suitable ranges of nucleation undercooling and nuclei density values. The predicted CET positions are compared with the experimentally measured CET position. Reasonable agreement is found at low levels of nuclei density. The paper concludes with estimates for the solidification conditions (nuclei density and nucleation undercooling) that led to the CET.

1. Introduction

Gamma titanium aluminide (γ–TiAl or TiAl) alloys are of interest to the aerospace and automotive industries on account of their low density and good mechanical properties at high temperature [1][2]. Applications for TiAl alloys include (in aircraft engines): low pressure turbine (LPT) blades, stator vanes, and radial diffusers; and (in motorcar engines): turbocharger rotors and valve trains [3]. Currently, a 2nd generation TiAl alloy is in service in the LPT of General Electric's 'GEnx' aero-engine which is used to power Boeing's 787 Dreamliner aircraft [4]. Rising fuel costs have motivated further development of 3rd generation TiAl alloys so that the maximum application temperature is increased from 700 °C (for 2nd generation TiAl) to 850 °C by using higher quantities of molybdenum and niobium [5].

The alloy: Ti–45.5Al–4.7Nb–0.2C–0.2B (at. %)—referred to hereafter as alloy 455—is part of this study to investigate Columnar to Equiaxed Transition (CET) in transient directional solidification experiments carried out in a Bridgman furnace where traditional Bridgman solidification was combined with the power down method [6]. CET refers to the growth of columnar dendrites in a casting that are subsequently blocked by the nucleation and growth of equiaxed dendrites. CET is an unwanted phenomenon in cast components since two distinct microstructures may lead to discontinuous mechanical properties.

Hunt [7] provides an analytical model for predicting CET in steady-state directional solidification. CET is predicted to occur at a critical temperature gradient, the calculation of which is based on dendrite growth kinetics and, ultimately, nucleation undercooling and the number of heterogeneous nuclei per unit volume in the alloy melt. The Hunt model can be used to create a 'CET map' of growth

rate versus temperature gradient. Previous studies [8][9][10] have applied transient modelling data to Hunt CET maps to examine the location and solidification conditions that can lead to CET.

In this article, Hunt's analytical model is applied in a parametric study that examines the effect of various levels of nucleation undercooling and number of nuclei per unit volume on the critical temperature gradient for CET. The applied model incorporates the same growth kinetics as the numerical model used to simulate columnar growth in the power down experiment that yielded a CET in alloy 455. The numerical model result, specifically, the locus of growth rate and temperature gradient at the columnar front, is superimposed on CET maps determined using the Hunt model. The intersection of the locus plot with the CET map provides an estimate for the position of CET. Suitable combinations of nucleation undercooling and nuclei density that satisfy the experimentally measured CET position are then determined.

2. Methodology

2.1. Directional solidification experiments using a gamma TiAl alloy

Lapin et al. [6] provide a detailed description of directional solidification experiments carried out in a Bridgman furnace using alloy 455. A brief description of these experiments is provided here.

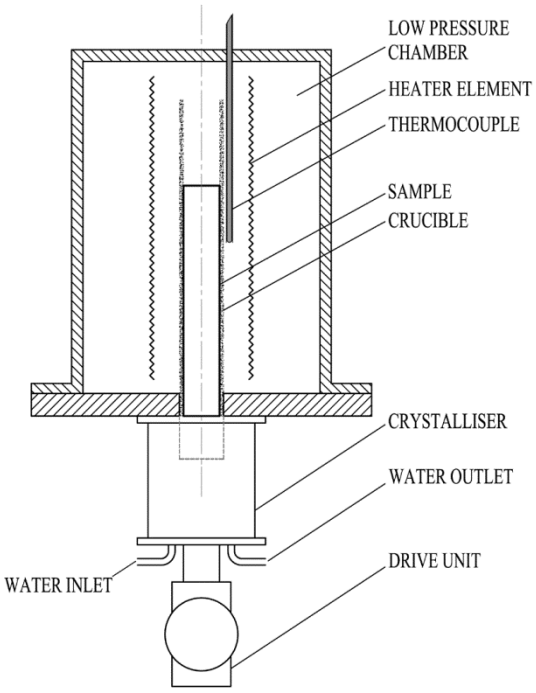

Figure 1. Schematic of the Bridgman furnace apparatus used in the power down experiment.

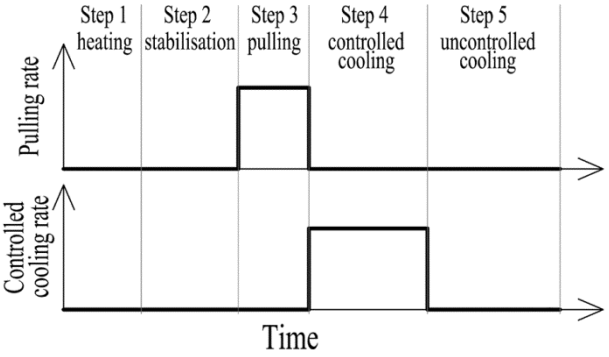

Figure 2. Typical pulling rate and controlled cooling rate signals plotted against time for each step in the experiment procedure.

Figure 1 shows a schematic drawing of the furnace arrangement. Figure 2 shows a plot of pulling rate and controlled cooling rate versus time for each step of the experimental procedure. In these experiments, traditional Bridgman solidification was combined in series with the power down method. The cylindrical sample (150 mm in length and 10 mm in diameter) was initially located in the furnace as shown in figure 1, i.e., its base was aligned with the top of the water-cooled crystalliser. The sample was heated (in Step 1) until the thermocouple read 1720 °C, and allowed to stabilize for 300 s (in Step 2). To induce directional columnar growth, the sample was pulled a distance of 20 mm over at time of 72 s into the crystalliser (in Step 3, Bridgman solidification). Next, controlled cooling began (in Step 4, power down method) at a predefined cooling rate, as measured by the thermocouple, until the entire

sample was solidified. The sample was then allowed to cool to room temperature without control (in Step 5). Four experiments were carried out at controlled cooling rates of 15, 20, 30 and 50 °C/min. The results for the sample cooled at 30 °C/min are of interest in this paper.

2.2. Numerical model (for columnar growth)

A hybrid one-dimensional thermal model of solidification, known as the Bridgman Furnace Front Tracking Model (BFFTM) [11], is applied. This model uses an explicit finite difference control volume (CV) method to solve the following heat equation (adapted from [12] and [13]) for temperature in a cylindrical rod of cross-sectional area A, and perimeter p, moving in the axial (x) direction at a pulling rate u,

$$\frac{\partial}{\partial t}(\rho c T) = \frac{\partial}{\partial x}\left(k\frac{\partial T}{\partial x}\right) - u\rho c\frac{\partial T}{\partial x} - \frac{hp}{A}(T - T_\infty) + E \quad , \tag{1}$$

where ρ, c and k are the density, specific heat capacity and thermal conductivity of the rod material, respectively; T_∞ is the temperature of the surrounding heat source (or sink), h is the heat transfer coefficient at the circumference of the rod, and E is the latent heat generated per unit volume. The CVs are disc-shaped so that the numerical domain fully encompasses the sample. In this way, radial heat flow from the heat source (in the hot zone) or to the heat sink (in the cold zone) is accounted for. The heat transfer coefficients were estimated as a function of axial position through a dedicated characterization study [14] of the same furnace used in the experiments described above.

The growth of columnar grains in alloy 455 is estimated using the dendrite growth model of Kurz et al. [15] (KGT model) using the liquidus slope and partition coefficient of a constitutionally similar binary alloy, namely: Ti–46at.%Al, (after Rebow et al. [16]). Using this approach, the following power law curve fit relates columnar growth rate (v_{tip}) to columnar dendrite tip undercooling (ΔT_{tip}): $v_{tip}=C(\Delta T_{tip})^b$, where $C = 2.63\times10^{-6}$ m/s·°C^b and $b = 2.79$. Latent heat release is calculated based on a Thermocalc [17] prediction for solid fraction versus temperature in the full multicomponent alloy, details of which can be found in reference [14]. The solidification conditions at the columnar dendrite tip can be estimated using the model, for example, columnar tip growth rate, temperature and temperature gradient. Since the front position is tracked and the thermal profile is known, it is also possible to estimate the extent of constitutionally undercooled liquid ahead of the front, i.e., the difference between the front position and the position of the equilibrium liquidus temperature isotherm.

2.3. Analytical model (for CET)

Hunt [7] presents a 1-dimensional analytical model that predicts columnar, equiaxed or mixed microstructure for steady-state directional solidification using the Bridgman method. An analysis is presented that uses an intuitive approach to calculate the extended volume fraction of equiaxed grains. The model predicts 'fully equiaxed' growth when,

$$G_{tip} < 0.617 N_0^{1/3}\left\{1 - \frac{(\Delta T_n)^3}{(\Delta T_{tip})^3}\right\}\Delta T_{tip} \quad , \tag{2}$$

where G_{tip} is the temperature gradient at the columnar dendrite tip, N_o is the nuclei density, i.e., the total number of available heterogeneous substrate particles per unit volume, ΔT_n is the nucleation undercooling, and ΔT_{tip} is the columnar dendrite tip undercooling. In Hunt's analysis, ΔT_{tip} is calculated via an empirical function of growth rate, v_{tip}, after Burden and Hunt [18]. The above expression is derived from an assumption based on a probabilistic analysis of columnar and equiaxed grain geometry, where 'fully equiaxed' growth corresponds to an extended volume fraction of equiaxed grains equal to 0.66, and 'fully columnar' growth corresponding to volume fraction of equiaxed grains equal to 1% of this value. The results of the analysis are presented in plots of columnar growth rate versus temperature gradient (known as CET maps), showing the predicted equiaxed, mixed (equiaxed and columnar), and fully columnar regions for a given alloy composition, nuclei density and nucleation undercooling. Hunt concludes the analysis stating that, at low growth

rates equiaxed growth depends on the efficiency of grain refiners, and that, at high temperature gradients the number of nucleation sites is more important.

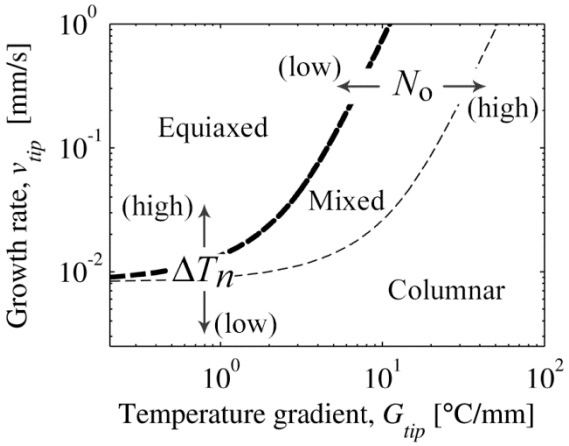

Figure 3. A CET map produced using the Hunt model [7]; the effect of using high and low values for nucleation undercooling (ΔT_n) and nuclei density (N_o) is shown.

This result is illustrated in the CET map shown in figure 3. The thick dashed line is a plot of G_{tip}, calculated from equation (2), over a range of growth rates, while the thin dashed line is a plot of G_{tip} for the 'fully columnar' case. Any combination of growth rate and temperature gradient in the area above the thick line is expected to produce fully equiaxed microstructure and, similarly, any combination of these values in the area below the thin line should produce a fully columnar microstructure. In between these lines a mixed equiaxed and columnar microstructure is expected. High values of N_o tend to shift the plots to the right and low values shift the plots to the left; whereas high values of ΔT_n shift the y-axis intercept of each plot upwards and low values shift the y-axis intercept downwards. The above described criterion for CET has become known as *mechanical* blocking [19] and is currently the most widely used in the literature [20].

3. Results

In a previous study by Mooney et al. [21], optical microscopy was used to reveal the primary β-phase (dendritic) microstructure in the four samples from the directional solidification experiments described in Section 2.1. A CET was discovered in the sample cooled at a rate of 30 °C/min. A microstructural analysis (for all samples), along with numerical modelling results using the model described in Section 2.2, is provided.

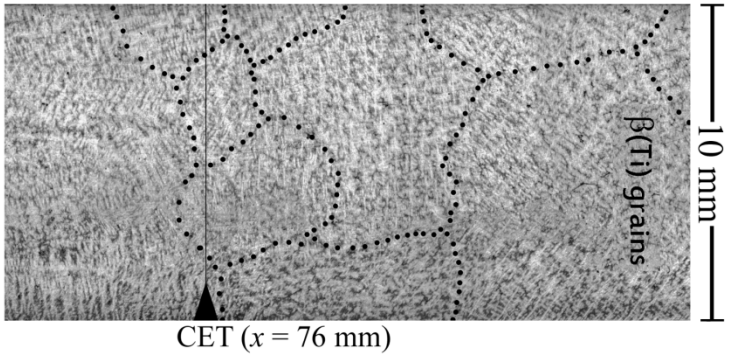

Figure 4. Section image of the CET (at x = 76 mm) given by the primary β-phase microstructure from the sample cooled at 30 °C/min in directional solidification experiments [6] using alloy 455, reproduced from a study by Mooney et al. [21].

For the purposes of this article, we are concerned with the microstructural analysis, specifically, the CET position, and numerical modelling results from reference [21] for the sample that contained the CET only. Figure 4 shows a section image of the sample that contained the CET. The CET was measured at an axial position of 76 mm.

3.1. Numerical modelling results

Figure 5 shows a plot—obtained using the numerical BFFTM—of the locus of growth rate and temperature gradient at the columnar front, with annotations showing the position of the columnar front in the sample. In this plot, the local peak (at a front position of approximately 25 mm) corresponds to the end of the Bridgman stage of the procedure (step 3) and the beginning of power down solidification stage (step 4). The simulation is valid up to the position of CET (at 76 mm) since only columnar growth is simulated. At this location the simulated growth rate was 0.128 mm/s, the temperature gradient was 1.089 °C/mm, and the tip undercooling was 4 °C.

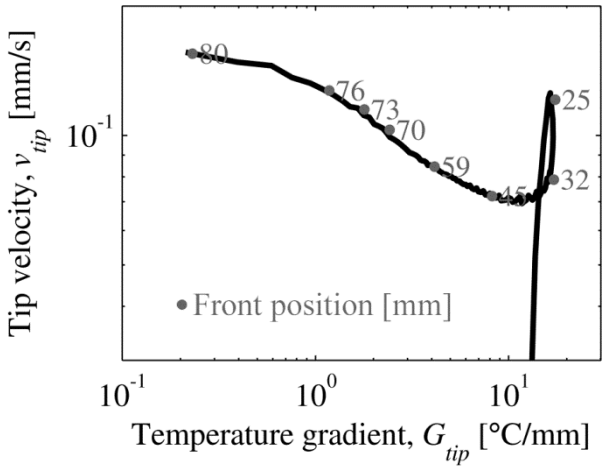

Figure 5. Simulated locus plot of columnar tip growth rate versus columnar tip temperature gradient for the sample solidified at a controlled cooling rate of 30 °C/min.

3.2. Analytical modelling results

CET maps were produced using the Hunt model for a range of combinations of nucleation undercooling values (from 0 °C to 4 °C) and nuclei densities (within a range from 0.01 /mm^3 to 100 /mm^3); 45 CET datasets were produced in total. The KGT dendrite growth kinetics model for alloy 455 was used to relate the columnar dendrite tip growth rate to ΔT_{tip} in the Hunt model. In effect a

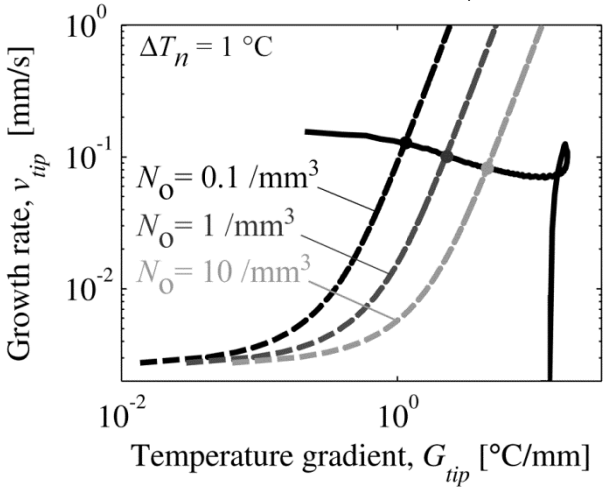

Figure 6 CET maps using the Hunt–KGT model and locus plot from the numerical model.

'Hunt–KGT' model is implemented.

Figure 6 shows three CET curves {given by equation (2) with ΔT_n = 1 °C} where the nucleation density varies between three levels: N_o=0.1, 1 and 10 /mm^3. The numerically estimated locus of temperature gradient, G_{tip}, and growth rate, v_{tip}, at the columnar front, from figure 5, is superimposed onto figure 6. The intersection of the G_{tip}–v_{tip} locus with a CET curve provides a viable CET prediction based on the specific values for the parameters ΔT_n and N_o. Table 1 shows the results from this exercise for all combinations ΔT_n and N_o in the range of values given above.

Table 1. Predicted front positions for CET (in mm), given by the intersection of the locus of temperature gradient and growth rate at the columnar dendrite tip with the Hunt–KGT CET map, for various nucleation undercooling and nuclei density values.

N_o [/mm^3]	Nucleation undercooling, ΔT_n [°C]								
	0	0.5	1.0	1.5	2.0	2.5	3.0	3.5	4.0
0.01	78.7	78.7	78.8	78.8	79.0	79.3	79.7	80.2	–
0.1	75.7	75.7	75.8	76.0	76.4	77.0	77.8	78.9	80.3
1	69.2	69.2	69.5	70.6	71.0	72.6	74.6	76.9	79.4
10	55.0	55.1	55.6	56.8	59.5	64.0	69.1	74.0	78.3
100	41.7	41.8	42.2	43.3	45.7	50.3	59.8	70.5	77.4

(We note that in the simulations detailed in reference [21], the columnar dendrite tip undercooling did not exceed 4 °C before the CET occurred; therefore we expect ΔT_n to be limited by this value.) Figure 7 shows the predicted CET positions from Table 1 plotted against nucleation undercooling for each nuclei density value; after Martorano et al. [22].

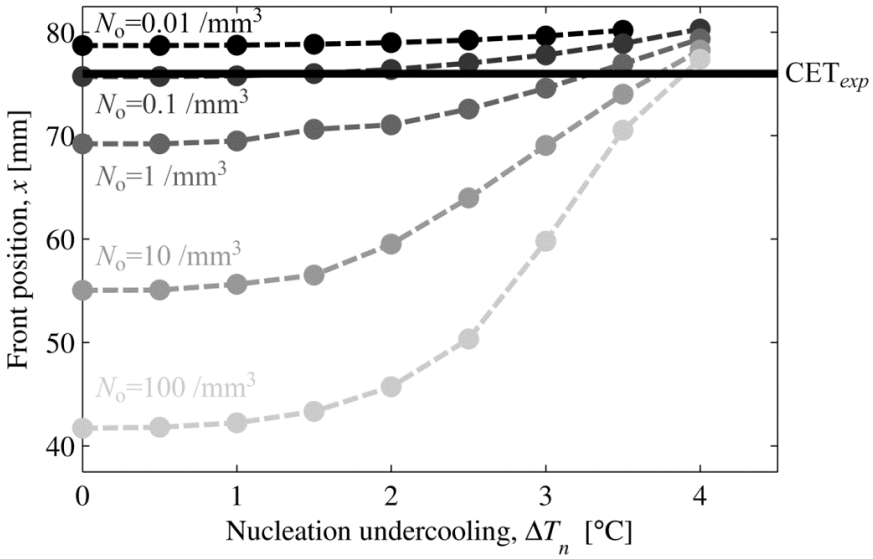

Figure 7. Predicted position of CET (dashed lines) using the Hunt–KGT model at various nucleation undercoolings and nuclei densities, and the measured CET position from the power down experiment.

4. Discussion

Figure 7 summarises the results in table 1. Each data point was calculated at the point of intersection of the BFFTM simulated G_{tip}–v_{tip} locus and the analytically calculated Hunt–KGT curve. In addition to these estimated CET locations, the measured CET location is shown at x = 76mm. At a value of N_o = 0.1 /mm^3 there is agreement with the experimentally measured CET position in the range of nucleation

undercoolings between 0 °C to 2 °C. At the lower value of N_o = 0.01 /mm^3, the predicted CET is slightly overestimated for all nucleation undercoolings up to 4 °C. At higher values of N_o (N_o = 1 /mm^3 and greater) there is agreement with the measured CET position, however, agreement occurs at specific values of nucleation undercooling, for example, with N_o=10 /mm^3 agreement occurs ΔT_n=3.7 °C. In any case, we can practically rule out high values for N_o since the alloy used in the experiment was not deliberately inoculated.

Following these results, a nuclei density of 0.1 /mm^3 is a reasonable estimate for alloy 455, as it suggests that nucleation undercooling was of the order of 2 °C. The Hunt CET maps for a nucleation density of 0.1 /mm^3, over a range of nucleation undercoolings, are shown in figure 8 (a) and (b). Exact agreement is found when ΔT_n has a value of 1.5 °C.

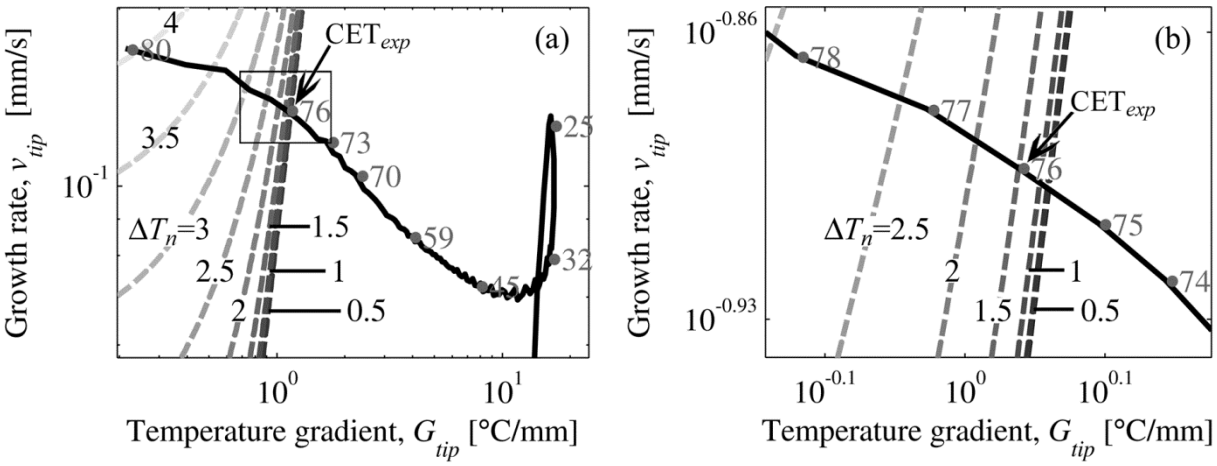

Figure 8. (a) CET maps (dashed lines) using the Hunt–KGT model where the nuclei density is set to 0.1 /mm^3 at various nucleation undercooling values, and superimposed locus plot (solid line) from the numerical model with the front position values (grey text) shown in mm. A portion (black rectangle) of this plot is enlarged in part (b) of this figure.

The BFFTM is appropriate for low Biot number (*Bi*) scenarios, specifically, where *Bi*<0.1. The Biot number was 0.03 or less in the simulations presented here. This means that the temperature at the center of the rod was very nearly equal to the temperature at its circumference. The numerical model does not treat convection in the melt. Since we are using a vertical Bridgman furnace, the density gradient is parallel with the gravity vector and, therefore, has a stabilising effect on the melt. Any solutal gradient in the melt that may have a destabilising effect is not treated in the current model. Further discussion on the assumptions of the numerical model can be found in reference [14].

5. Conclusions

The performance of an experimental apparatus was simulated using a numerical model and the simulated results were compared to those from an analytical model for CET. The CET position was measured from the final microstructure and a reasonable estimate of the nucleation parameters was obtained. The main outcomes from this study are outlined below:

- A combined Bridgman, power-down experiment was conducted on a gamma TiAl alloy [6] and a CET was observed when the cooling rate in the power-down phase was 30 °C/min.
- A Bridgman Furnace Front Tracking Model was applied to the experiment and this allowed the transient thermal history to be predicted by simulation.
- Hunt's analytical model for CET [7] with KGT dendritic growth kinetics was applied.

- Using the Hunt–KGT model, a parameters variation analysis focused on a range of nucleation undercooling (ΔT_n=0 °C to 4 °C) and nuclei density (N_o=0.01 /mm^3 to 100 /mm^3) values.
- The locus of growth rate and temperature gradient, given by the numerical simulation, was superimposed onto the CET curves from the Hunt–KGT model. The intersection of the locus with individual CET curves gave the predicted position of CET for each combination of ΔT_n and N_o.
- The predicted CET positions were compared with the experimentally measured CET location.
- A nuclei density of the order of 0.1 /mm^3 gave reasonable agreement between the experiment and model results over a range of nucleation undercooling from 0 °C to 2 °C.

Acknowledgments
This work was carried out as part of the GRADECET (GRAvity DEpendence of Columnar to Equiaxed Transition in TiAl Alloys) research project. The authors (R. P. Mooney and S. McFadden) thank the European Space Agency PRODEX programme for funding the research (agreement number: 4000107132) under the management of the Irish Space Delegation at Enterprise Ireland. The authors (J. Lapin and A. Klimová) acknowledge the financial support of the Slovak Grant Agency for Science under the contract VEGA 2/0149/13 and the Slovak Academy of Sciences under the contract of MVTS funding of ESA project GRADECET. Finally, the authors would like to acknowledge U. Hecht and L. Sturz of ACCESS e.V, Aachen, for their interesting and helpful comments on this paper.

References
[1] Loria E A 2000 *Intermetallics* **8** 9–11 1339–1345
[2] Dimiduk D M 1999 *Mater. Sci. Eng. A* **263** 2 281–288
[3] Appel F, Paul J D H and Oehring M 2011 *Gamma Titanium Aluminide Alloys: Science and Technology*
[4] Bewlay B P, Weimer M, Kelly T, Suzuki A and Subramanian P R 2013 *MRS Proc.* **1516** 49–57
[5] Clemens H and Smarsly W 2011 *Adv. Mater. Res.* **278** 551–556
[6] Lapin J, Gabalcová Z, Hecht U, Mooney R P and McFadden S 2014 *Mater. Sci. Forum* **790–791** 193–198
[7] Hunt J D 1984 *Mater. Sci. Eng.* **65** 1 75–83
[8] Kartavykh A V, Ganina S, Grothe D, Lemoisson F and Herfs W 2010 *Mater. Sci. Forum* **649** 223–228
[9] McFadden S, Browne D J, Sturz L and Zimmermann G 2010 *Mater. Sci. Forum* **649** 361–366
[10] Murphy A G, Reinhart G, Nguyen-Thi H, Abou Jaoude G S and Browne D J 2013 *J. Alloys Compd.* **573** 170–176
[11] Mooney R P, McFadden S, Rebow M and Browne D J 2012 *Trans. Indian Inst. Met.* **65** 6 527–530
[12] Carslaw H S and Jaeger J C 1959 *Conduction of Heat in Solids* 2nd ed.
[13] Bejan A 1993 *Heat Transfer* 1st ed.
[14] Mooney R P, McFadden S, Gabalcová Z and Lapin J 2014 *Appl. Therm. Eng.* **67** 1–2 61–71
[15] Kurz W, Giovanola B and Trivedi R 1986 *Acta Metall.* **34** 5 823–830
[16] Rebow M, Browne D J and Fautrelle Y 2010 *Mater. Sci. Forum* **649** 243–248
[17] Thermo-Calc Software AB 20132013. [Online]. Available: http://www.thermocalc.com/Thermo-Calc.htm
[18] Burden M H and Hunt J D 1974 *J. Cryst. Growth* **22** 2 99–108
[19] Dong H B and Lee P D 2005 *Acta Mater.* **53** 3 659–668
[20] Spittle J A 2006 *Int. Mater. Rev.* **51** 4 247–269
[21] R P Mooney U Hecht Z Gabalcová J Lapin and S McFadden 2015 *Kov. Mater.* **53** 3 187
[22] Martorano M A, Beckermann C and Gandin C- A 2003 *Metall. Mater. Trans. A Phys. Metall. Mater. Sci.* **34 A** 8 1657–1674